

Physics-Informed Neural Networks for Chemotherapy Pharmacokinetics: Benchmarking the Clinical Estimator and Exposing Parameter Identifiability

Riya Bisht* Dhruv Agarwal†

May 31, 2026

Abstract

Physics-Informed Neural Networks (PINNs) are an attractive tool for *partial-observation* problems in biology, where the governing dynamics are known but some compartments cannot be measured. Chemotherapy pharmacokinetics (PK) is a clean instance: drug concentration in plasma is routinely measured, but concentration in tissue—which determines tumour kill and off-target toxicity—is not. We benchmark a PINN against the standard clinical baseline (nonlinear least-squares on the analytical biexponential plasma solution, hereafter NLS) and a physics-agnostic neural baseline (a data-only MLP) on two PK problems. On the **linear two-compartment** problem, NLS is near-optimal; the PINN matches it to within a small constant factor while also producing the tissue curve in a single training pass, whereas the data-only MLP fails on tissue by roughly $10\times$. On a **Michaelis–Menten** extension (saturable elimination), the biexponential closed form no longer exists, so NLS is mis-specified and silently returns meaningless rate constants. The PINN instead exposes a deeper fact: the Michaelis–Menten two-compartment model is *non-identifiable from plasma alone*, and the PINN reports this honestly by converging to a basin with $k_{12} \rightarrow 0$. Adding **two sparse tissue observations** largely resolves identifiability: across five seeds the PINN recovers k_{21} to within 1% of truth and V_{\max}, K_m to within one standard-deviation bar, while k_{12} moves in the correct direction ($0.02 \rightarrow 0.82$) but remains $\sim 2\sigma$ below truth—a recovery the closed-form NLS estimator cannot attempt at all, because its biexponential ansatz describes only plasma. Our claim is *not* that PINNs beat NLS. It is that PINNs offer a uniform recipe that ties the textbook estimator on the textbook problem, exposes structural identifiability that the textbook estimator hides, and absorbs heterogeneous measurements within a single loss.

1 Introduction

Chemotherapy dosing is fundamentally a question of *concentration over time, at the right place*. Plasma concentration is observable through blood sampling; tissue (and tumour) concentration is generally not observable in patients. Compartmental PK models therefore play a double role: (i) summarising plasma data and (ii) inferring the unobserved compartments where the drug actually acts.

*manasi.riya2003@gmail.com

†dhruvagarwal5018@gmail.com

The standard estimator in clinical PK is nonlinear least-squares on a biexponential plasma function, derived analytically from the linear two-compartment ODE. It works extremely well when its assumptions hold (linear kinetics, well-characterised input, modest noise) and poorly when they do not (saturable enzymes, time-varying input, structural extensions).

PINNs (Raissi et al., 2019) offer an alternative formulation: rather than solve the ODE symbolically and fit its closed form, we train a neural network to satisfy the ODE in the sense of a *residual*, evaluated by automatic differentiation at collocation points. Three things become easy: nonlinear and structural extensions are a one-line change to the residual; hidden compartments are returned by the same network that fits the observed compartment; and the known initial condition (the dose) is enforced as a loss term rather than a fitted parameter. This paper sets up the fairest possible comparison between the two approaches and reports the numbers honestly. We do not propose a new architecture, loss, or optimiser; our contribution is a careful, multi-seed benchmark and one identifiability observation we believe is usefully framed.

2 Related work

PINNs were introduced by Raissi et al. (2019) for forward and inverse problems in differential equations, building on earlier neural ODE/PDE solvers (Lagaris et al., 1998); Karniadakis et al. (2021) and Cuomo et al. (2022) survey the now-large physics-informed and scientific machine-learning literature, and mature software such as DeepXDE (Lu et al., 2021) has lowered the cost of applying the recipe. A central appeal for our setting is inverse inference of *unobserved* fields: Raissi et al. (2020) recover hidden velocity and pressure from partial flow observations, and Yazdani et al. (2020) infer unobserved species and unknown parameters in biological reaction networks from sparse, noisy measurements—the systems-biology analogue of recovering an unmeasured tissue compartment from plasma. PINN training is, however, known to be delicate—loss landscapes admit poor basins and stiff-gradient pathologies (Wang et al., 2022)—which is precisely the lens through which we read the $k_{12} \rightarrow 0$ solution below: not an optimiser failure, but the basin the data actually support.

Applications of PINNs to compartmental pharmacokinetics are now a rapidly growing area. Recent work embeds compartmental ODEs—including fractional-order and time-varying-rate extensions—in the PINN residual to discover drug dynamics (Ahmadi Daryakenari et al., 2025, 2024; Nasim & Nasim, 2024), learns unknown reaction terms in chemotherapy PK/PD models such as doxorubicin cell-kill via universal PINNs (Podina et al., 2025), estimates population-level parameter *distributions* from aggregated concentration data with a distributional PINN benchmarked against MCMC (Tsiros et al., 2026), and performs inverse parameter estimation in physiologically-based (PBPK) models benchmarked against classical estimators (Wickramasinghe et al., 2025). Relative to this line, our setting is deliberately minimal—a two-compartment model with a closed-form plasma solution—which lets us run a comparison that is still uncommon: a like-for-like, multi-seed benchmark of a *standard* PINN against the nonlinear least-squares biexponential estimator that clinical pharmacologists actually use (Gabrielsson & Weiner, 2016), rather than against a data-only neural network, an MCMC sampler, or an evolutionary optimiser alone. The closest existing comparison pits scientific-ML against population-PK and classical ML for concentration *prediction* (Valderrama et al., 2025); our focus is instead single-patient parameter identifiability and hidden-compartment recovery.

The structural and practical non-identifiability of (bio)compartmental ODE models from partial observations is itself long established (Bellman & Åström, 1970; Cobelli & DiStefano, 1980; Walter & Pronzato, 1997), including for nonlinear models in biology (Miao et al., 2011) and for nonlinear

(Michaelis–Menten) PK models specifically (Godfrey et al., 1994); the structural-versus-practical distinction is formalised by profile-likelihood analysis (Raue et al., 2009), and identifiability analysis has recently been coupled directly with PINN-style parameter estimation and gray-box identification in systems biology (Daneker et al., 2023; Ahmadi Daryakenari et al., 2024). Our contribution is not this fact but the qualitative observation that, on the Michaelis–Menten extension, a PINN *surfaces* non-identifiability directly—by converging to a $k_{12} \rightarrow 0$ basin—whereas the mis-specified closed-form estimator conceals it behind rate constants that do not apply to the true ODE. This differs in stance from methods that establish identifiability *a priori* and then constrain the PINN loss or model structure accordingly (Ahmadi Daryakenari et al., 2025; Daneker et al., 2023): we leave the fit unconstrained and read its collapse to the $k_{12} \rightarrow 0$ basin as the diagnostic itself. To our knowledge this framing, together with the like-for-like multi-seed comparison against the clinical estimator, has not been reported.

3 Background

3.1 The linear two-compartment model

After an instantaneous intravenous bolus of dose D distributed over plasma volume V_p , the linear two-compartment ODE is

$$\frac{dC_p}{dt} = -(k_e + k_{12}) C_p + k_{21} C_t, \quad (1)$$

$$\frac{dC_t}{dt} = k_{12} C_p - k_{21} C_t, \quad C_p(0) = D/V_p, \quad C_t(0) = 0, \quad (2)$$

with closed-form plasma solution $C_p(t) = Ae^{-\alpha t} + Be^{-\beta t}$, where $\alpha + \beta = k_e + k_{12} + k_{21}$, $\alpha\beta = k_e k_{21}$, and $A + B = C_p(0)$. The classical estimator fits (A, B, α, β) to plasma samples and inverts to (k_e, k_{12}, k_{21}) .

3.2 The Michaelis–Menten extension

When the eliminating enzyme saturates,

$$\frac{dC_p}{dt} = -\frac{V_{\max} C_p}{K_m + C_p} - k_{12} C_p + k_{21} C_t. \quad (3)$$

There is no biexponential closed form. The plasma curve decays roughly linearly in time when $C_p \gg K_m$ (zero-order, capacity-limited elimination) and roughly exponentially when $C_p \ll K_m$ (first-order). This regime change is the hallmark of saturable (capacity-limited) elimination, the textbook clinical example being phenytoin, whose clearance falls as concentration rises within the therapeutic range.

3.3 PINN formulation

The network $f_\theta : \mathbb{R} \rightarrow \mathbb{R}^2$ maps time to (\hat{C}_p, \hat{C}_t) . With ODE parameters θ_{phys} jointly trainable (stored as $\log \theta_{\text{phys}}$ to stay positive) and collocation points $\{t_c\}$ sampled from $[0, T]$, the loss is

$$L = L_{\text{data}} + \lambda_{\text{phys}} L_{\text{phys}} + \lambda_{\text{ic}} L_{\text{ic}}, \quad (4)$$

with $L_{\text{data}} = \text{mean}_{t \in \text{obs}} (\hat{C}_p(t) - C_p^{\text{obs}}(t))^2$, $L_{\text{ic}} = (\hat{C}_p(0) - C_p(0))^2 + \hat{C}_t(0)^2$, and L_{phys} the mean-squared ODE residual for both states, with $d\hat{C}/dt$ from `autograd`. Switching between the linear and Michaelis–Menten residual is a two-line edit.

4 Method

Architecture. A small fully-connected network suffices: 4 hidden layers \times 64 units, tanh activations, and a `softplus` output to enforce non-negative concentrations ($\sim 13\text{k}$ parameters).

Losses and weights. $\lambda_{\text{phys}} = 5$, $\lambda_{\text{ic}} = 20$. The IC weight is high because the dose is known exactly; the physics weight is set so the physics and data terms are comparable in magnitude after a few hundred Adam steps. Results are insensitive to $\lambda_{\text{phys}} \in [1, 20]$.

Two-stage optimisation. Standard PINN practice: Adam (Kingma & Ba, 2015) for global exploration (6000–8000 steps, lr 5×10^{-3} , 200 collocation points resampled each step—70% uniform on $[0, 24]$, 30% concentrated on $[0, 4]$ where the dynamics are fast), then L-BFGS (Liu & Nocedal, 1989) with strong-Wolfe line search (up to ~ 300 iterations on a fixed 160-point grid). Wall-clock per PINN run is ~ 20 –30s on a single CPU core; the whole benchmark finishes in under an hour on a laptop.

Baselines. **NLS:** `scipy.optimize.curve_fit` (Levenberg–Marquardt) on $C_p(t) = (C_{p0} - B)e^{-\alpha t} + Be^{-\beta t}$, fixing $A + B = C_{p0}$ (known dose), then inverting $(A, B, \alpha, \beta) \rightarrow (k_e, k_{12}, k_{21})$ and integrating the ODE for the tissue curve. **MLP:** identical network and optimiser to the PINN, plasma data only, no physics term and no tissue supervision—this isolates the contribution of the physics prior.

Data. Synthetic ground truth from `scipy.integrate.odeint` on a 481-point grid over $[0, 24]$ hours. Sparse plasma samples are drawn at evenly spaced times in $[0.5, 24]$ h and corrupted with multiplicative Gaussian noise ($C_p^{\text{obs}} = C_p^{\text{true}}(1 + \varepsilon)$, $\varepsilon \sim \mathcal{N}(0, \sigma^2)$, clipped to ≥ 0). Reference parameters are in the published range for doxorubicin ($k_e = 0.5$, $k_{12} = 1.0$, $k_{21} = 0.4$, $V_p = 25$ L, $D = 50$ mg).

5 Experiments

We run three linear-ODE experiments at five seeds each (mean \pm std reported throughout): a *headline* run ($n = 8$, $\sigma = 10\%$); a *noise sweep* ($\sigma \in \{1, 5, 10, 20\}\%$, $n = 8$); and a *sparsity sweep* ($n \in \{4, 6, 8, 12, 20\}$, $\sigma = 10\%$). We then run a structural-misspecification experiment in which data is generated by the Michaelis–Menten ODE and all three methods are applied. All raw runs are released with the code.

6 Results

6.1 Headline: linear ODE

Table 1 should be read honestly: NLS and PINN are statistically tied on every metric (differences within one std bar across five seeds). NLS recovers k_e both more cleanly and with less bias—the PINN is marginally biased high (0.520 vs. true 0.500)—because it is the maximum-likelihood estimator on a correctly-specified model; the PINN pays a $\sim 6000\times$ wall-clock penalty for the otherwise-equivalent answer. The physics-agnostic MLP, with identical capacity, is $\sim 10\times$ worse on

Table 1: Headline linear-ODE result ($n = 8$ samples, $\sigma = 10\%$, 5 seeds). Best value per column in bold. RMSE in mg/L.

Method	RMSE C_p	RMSE C_t	k_e (0.50)	k_{12} (1.00)	k_{21} (0.40)	Wall-clock
NLS	0.016 ± 0.017	0.031 ± 0.025	0.493 ± 0.013	0.921 ± 0.215	0.368 ± 0.090	0.004 s
PINN	0.017 ± 0.017	0.039 ± 0.031	0.520 ± 0.018	0.883 ± 0.208	0.361 ± 0.064	25.1 s
MLP	0.071 ± 0.020	0.355 ± 0.111	—	—	—	9.2 s

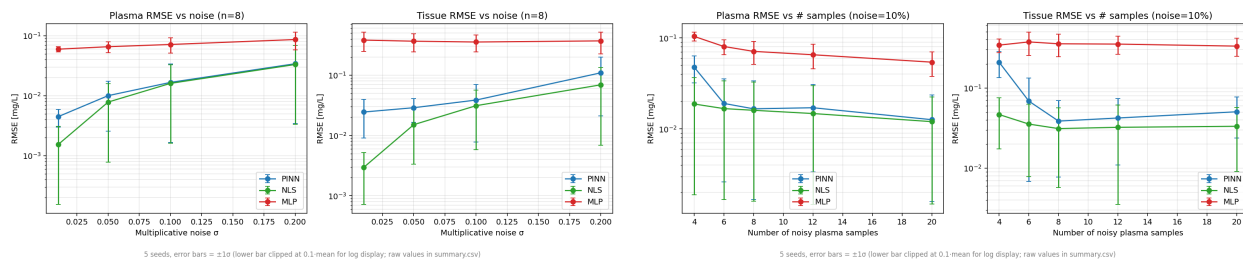


Figure 1: Tissue RMSE (mg/L, log scale, error bars over 5 seeds) versus noise level (left) and plasma sample count (right). NLS and PINN track each other on the well-specified linear problem; the data-only MLP is flat and far above both.

the hidden tissue compartment and $\sim 4\times$ worse on plasma—that gap is the clean PINN-vs-no-prior demonstration. The large std on k_{12} for both estimators is a *practical* (conditioning) effect, not a structural one: given the known dose the linear two-compartment model is structurally identifiable from plasma alone—in the noise-free limit the biexponential inversion $k_{21} = (A\beta + B\alpha)/(A + B)$, $k_e = \alpha\beta/k_{21}$, $k_{12} = \alpha + \beta - k_e - k_{21}$ recovers (k_e, k_{12}, k_{21}) exactly—but k_{12} is by far the most poorly conditioned of the three at realistic noise, because it is obtained only as a difference of comparably-sized quantities (Raue et al., 2009). This is a property of the data, not a flaw of either method.

6.2 Noise and sparsity robustness

Figure 1 summarises tissue-RMSE behaviour across noise levels and sample counts (full tables in Appendix A). NLS scales tightly and essentially linearly with noise, as expected for a correctly-specified linear estimator. The PINN scales similarly with a slightly higher floor at low noise (the physics residual caps how aggressively it fits individual plasma points); at realistic clinical noise ($\geq 10\%$) the two are within one std bar. The PINN is within $\sim 1.5\times$ of NLS for $n \geq 8$ and degrades at $n = 4$, where the network has more capacity than the data can constrain. The MLP tissue error is roughly flat regardless of noise or sample count—there is no information about tissue in plasma samples without a physics prior to propagate it.

6.3 Misspecification and identifiability (Michaelis–Menten)

This experiment exposes the *structural* difference between the methods. Data is generated from the Michaelis–Menten ODE ($V_{\max} = 1.5$ mg/L/hr, $K_m = 0.3$ mg/L, $k_{12} = 1.0$, $k_{21} = 0.4$).

Finding 1 — NLS is mis-specified. The biexponential closed form NLS fits does not exist for a Michaelis–Menten ODE. NLS returns the best biexponential approximation to plasma; the inverted

Table 2: Michaelis–Menten RMSE (mg/L, 5 seeds, $n = 8$ plasma observations).

Method	Plasma RMSE	Tissue RMSE
NLS biexp (mis-specified)	0.025 ± 0.013	0.166 ± 0.012
MLP (data only)	0.091 ± 0.002	0.492 ± 0.164
PINN, plasma only	0.026 ± 0.003	0.215 ± 0.004
PINN + 1 tissue sample	0.021 ± 0.006	0.330 ± 0.072
PINN + 2 tissue samples	0.015 ± 0.012	0.028 ± 0.001

Table 3: Recovered Michaelis–Menten parameters (5 seeds). True values in parentheses.

Method	V_{\max} (1.50)	K_m (0.30)	k_{12} (1.00)	k_{21} (0.40)
PINN, plasma only	3.16 ± 0.18	0.50 ± 0.07	0.02 ± 0.02	0.19 ± 0.01
PINN + 1 tissue	2.52 ± 0.53	0.64 ± 0.06	0.59 ± 0.09	0.06 ± 0.01
PINN + 2 tissue	1.91 ± 0.46	0.37 ± 0.10	0.82 ± 0.09	0.40 ± 0.05

“linear” rate constants are meaningless and the propagated tissue curve has the wrong shape (peak $\sim 3\times$ too low).

Finding 2 — the PINN with plasma alone is non-identifiable. The PINN matches the plasma curve well (RMSE $\sim 26 \mu\text{g/L}$) but does so by setting $k_{12} \approx 0$ and inflating V_{\max} , yielding an essentially zero tissue curve. This is wrong, but it is *consistent with the plasma observations*: with $k_{12} = 0$ no drug reaches tissue and plasma must clear through V_{\max} alone. With four free parameters and one observable compartment, the system is locally non-identifiable in this regime: as $k_{12} \rightarrow 0$ the tissue compartment decouples from plasma, so plasma data carry essentially no information about k_{12} and the Fisher information matrix degenerates at this boundary. The PINN faithfully reports the answer the data actually supports; NLS hides the same gap behind rate constants that do not apply to the true ODE. We demonstrate this empirically rather than prove it; a formal treatment via the Fisher information matrix, profile likelihood (Raue et al., 2009), or a structural-identifiability analysis of the nonlinear model (Cobelli & DiStefano, 1980; Godfrey et al., 1994) is left to future work.

Finding 3 — sparse heterogeneous data resolves identifiability. Adding tissue measurements to the PINN loss is a one-line change. The *closed-form* NLS estimator cannot absorb a tissue measurement, because its biexponential ansatz describes only plasma. A numerical least-squares fit of the full ODE system could in principle absorb tissue data; doing so abandons the closed-form clinical estimator and amounts to a non-neural version of the same residual-fitting the PINN performs. Our point is therefore that the *standard clinical* biexponential estimator cannot, whereas the PINN does so with a one-line change. As Tables 2 and 3 show, one tissue sample (near the peak, $t = 1$ h) fixes the peak amplitude but not the decay; two tissue samples ($t = 1$ h and $t = 6$ h) constrain both branches, recovering k_{21} to within 1% of truth and V_{\max}, K_m to within one std bar across five seeds; k_{12} is recovered in the correct direction ($0.02 \rightarrow 0.82$) but remains $\sim 2\sigma$ below truth (Table 3). Figure 2 shows the “PINN + 2 tissue” curve overlaying ground truth almost exactly, while every other method fails in a characteristic way.

The take-away is *not* “PINN beats NLS.” It is that the PINN is a uniform framework that (a) ties the textbook estimator on the textbook problem, (b) exposes structural identifiability the textbook estimator hides, and (c) absorbs heterogeneous measurements—plasma points, one biopsy,

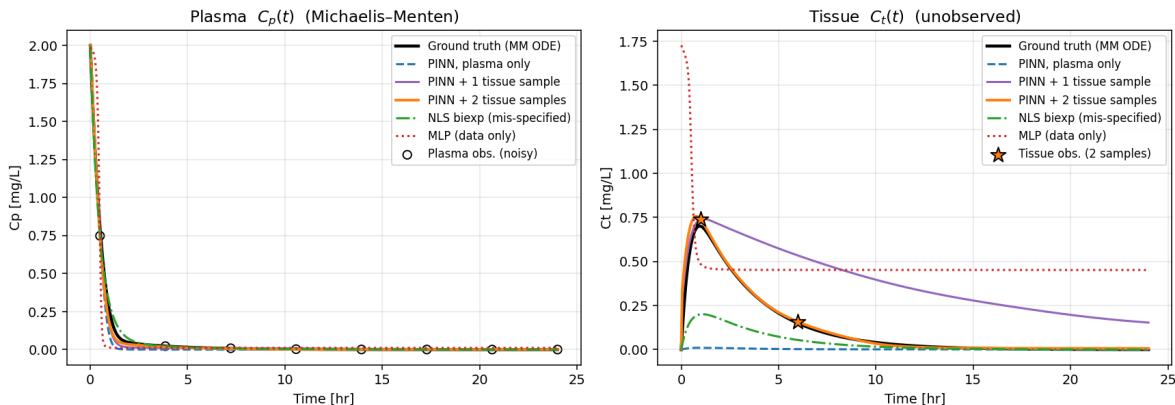


Figure 2: Michaelis–Menten tissue trajectories. The “PINN + 2 tissue” curve overlays the ground-truth tissue trajectory almost exactly; NLS (mis-specified), the data-only MLP, and the plasma-only PINN each fail differently. Plasma-only PINN collapses to near-zero tissue ($k_{12} \rightarrow 0$), the honest report of a non-identifiable fit.

a follow-up biopsy—within the same loss, recovering ground truth when the data are sufficient.

7 Discussion

What this benchmark says, and what it does not. PINNs are roughly competitive with the textbook PK estimator on the textbook PK problem, and meaningfully better when its assumptions break; they are dramatically better than physics-agnostic networks for inferring hidden states from partial observations. It does *not* say PINNs are the right tool when a closed-form estimator exists, problems are well-specified, and compute is the binding constraint—there, NLS is.

Identifiability. For the linear model, the plasma decay fixes the macro constants α, β and the amplitude split fixes k_{21} ; given the known dose ($A + B = C_{p0}$) the micro-constants (k_e, k_{12}, k_{21}) are then *structurally* identifiable from plasma, the noise-free inversion being exact. What is poor is the *conditioning*: k_{12} is recovered as a difference of comparable quantities, so its seed-to-seed variance is large for NLS and PINN alike. The PINN inherits this conditioning faithfully.

Cost. A PINN run is ~ 25 s on CPU; an NLS fit is instant. For 50,000-patient population studies this matters; for single-patient model exploration, teaching, or prototyping an extension, the absolute time is negligible.

Broader impact. The work is a methodological benchmark on synthetic data with no patient involvement. A positive impact is clearer, more honest inference of unobserved tissue exposure, which is the quantity that governs efficacy and toxicity; PINNs that expose identifiability gaps could reduce over-confident clinical inferences. The risk is the converse: any model that outputs unobserved tissue concentrations could be over-trusted in a dosing decision. We therefore stress that none of these methods is validated on real clinical data and none should inform patient care in its present form.

8 Limitations

- **Single noise model.** We use multiplicative Gaussian noise. Real assay noise is often heteroscedastic and includes lower-limit-of-quantification censoring, which neither baseline handles out of the box.
- **No inter-individual variability.** Real PK studies estimate population parameters with random effects (NONMEM, Monolix, Bayesian hierarchical models). All three methods here are individual-fit only.
- **Synthetic ground truth.** We have not tested on real clinical PK data; external validity requires refitting on a published dataset (e.g. the doxorubicin studies of Speth et al. (1988)).
- **No methodological novelty.** The architecture, loss, and optimisation recipe are standard (Raissi et al., 2019); the identifiability fact is long known in PK theory. Our contribution is the rigorous comparison and the framing, not a new method.

9 Future work

Natural extensions: (1) **PK/PD coupling**—add a tumour compartment with cell-kill proportional to $C_t \cdot N$, so the PINN jointly identifies PK and PD parameters while NLS would need a separate stage; (2) a **spatial PINN** (Krogh cylinder) using $\partial^2 C / \partial x^2$ from autograd for radial drug diffusion; (3) a **heteroscedastic/LLOQ-aware likelihood** replacing MSE with a censored-Gaussian negative log-likelihood; (4) a **population PINN** with per-patient parameter heads on a shared backbone; and (5) a **Bayesian PINN** (Yang et al., 2021) that turns the qualitative non-identifiability signal into calibrated posterior uncertainty on (k_{12}, V_{\max}, K_m) .

References

- Raissi, M., Perdikaris, P. & Karniadakis, G.E. (2019) Physics-informed neural networks: a deep learning framework for solving forward and inverse problems involving nonlinear partial differential equations. *Journal of Computational Physics* 378:686–707.
- Lagaris, I.E., Likas, A. & Fotiadis, D.I. (1998) Artificial neural networks for solving ordinary and partial differential equations. *IEEE Transactions on Neural Networks* 9(5):987–1000.
- Cuomo, S. et al. (2022) Scientific machine learning through physics-informed neural networks: where we are and what’s next. *Journal of Scientific Computing* 92:88.
- Gabrielsson, J. & Weiner, D. (2016) *Pharmacokinetic and Pharmacodynamic Data Analysis: Concepts and Applications*, 5th ed. Apotekarsocieteten.
- Speth, P.A.J., van Hoesel, Q.G.C.M. & Haanen, C. (1988) Clinical pharmacokinetics of doxorubicin. *Clinical Pharmacokinetics* 15(1):15–31.
- Cobelli, C. & DiStefano, J.J. (1980) Parameter and structural identifiability concepts and ambiguities: a critical review and analysis. *American Journal of Physiology* 239(1):R7–R24.
- Walter, E. & Pronzato, L. (1997) *Identification of Parametric Models from Experimental Data*. Springer.

- Karniadakis, G.E., Kevrekidis, I.G., Lu, L., Perdikaris, P., Wang, S. & Yang, L. (2021) Physics-informed machine learning. *Nature Reviews Physics* 3:422–440.
- Lu, L., Meng, X., Mao, Z. & Karniadakis, G.E. (2021) DeepXDE: a deep learning library for solving differential equations. *SIAM Review* 63(1):208–228.
- Raissi, M., Yazdani, A. & Karniadakis, G.E. (2020) Hidden fluid mechanics: learning velocity and pressure fields from flow visualizations. *Science* 367(6481):1026–1030.
- Wang, S., Yu, X. & Perdikaris, P. (2022) When and why PINNs fail to train: a neural tangent kernel perspective. *Journal of Computational Physics* 449:110768.
- Kingma, D.P. & Ba, J. (2015) Adam: a method for stochastic optimization. In *International Conference on Learning Representations (ICLR)*.
- Liu, D.C. & Nocedal, J. (1989) On the limited memory BFGS method for large scale optimization. *Mathematical Programming* 45(1–3):503–528.
- Bellman, R. & Åström, K.J. (1970) On structural identifiability. *Mathematical Biosciences* 7(3–4):329–339.
- Miao, H., Xia, X., Perelson, A.S. & Wu, H. (2011) On identifiability of nonlinear ODE models and applications in viral dynamics. *SIAM Review* 53(1):3–39.
- Yazdani, A., Lu, L., Raissi, M. & Karniadakis, G.E. (2020) Systems biology informed deep learning for inferring parameters and hidden dynamics. *PLOS Computational Biology* 16(11):e1007575.
- Daneker, M., Zhang, Z., Karniadakis, G.E. & Lu, L. (2023) Systems biology: identifiability analysis and parameter identification via systems-biology-informed neural networks. *Methods in Molecular Biology* 2634:87–105.
- Raue, A., Kreutz, C., Maiwald, T., Bachmann, J., Schilling, M., Klingmüller, U. & Timmer, J. (2009) Structural and practical identifiability analysis of partially observed dynamical models by exploiting the profile likelihood. *Bioinformatics* 25(15):1923–1929.
- Godfrey, K.R., Chapman, M.J. & Vajda, S. (1994) Identifiability and indistinguishability of nonlinear pharmacokinetic models. *Journal of Pharmacokinetics and Biopharmaceutics* 22(3):229–251.
- Ahmadi Daryakenari, N., Wang, S. & Karniadakis, G.E. (2025) CMINNs: compartment model informed neural networks—unlocking drug dynamics. *Computers in Biology and Medicine* 184:109392.
- Ahmadi Daryakenari, N., Wang, S. & Karniadakis, G.E. (2024) Pharmacometrics modeling via physics-informed neural networks: integrating time-variant absorption rates and fractional calculus for enhancing prediction accuracy. *arXiv preprint arXiv:2412.21076*.
- Nasim, I. & Nasim, A. (2024) Discovering intrinsic multi-compartment pharmacometric models using physics-informed neural networks. *arXiv preprint arXiv:2405.00166*.
- Podina, L., Ghodsi, A. & Kohandel, M. (2025) Learning chemotherapy drug action via universal physics-informed neural networks. *Pharmaceutical Research* 42(4):593–612.

- Tsiros, P., Minadakis, V. & Sarimveis, H. (2026) A physics-informed neural network approach for estimating population-level pharmacokinetic parameters from aggregated concentration data. *Journal of Pharmacokinetics and Pharmacodynamics* 53(2):11.
- Wickramasinghe, C.D., Weerasinghe, K.C., Ranaweera, P.K. & Hapuhinna, N.S.S.M. (2025) PBPk-iPINNs: inverse physics-informed neural networks for physiologically based pharmacokinetic brain models. *arXiv preprint arXiv:2509.12666*.
- Valderrama, D., Teplytska, O., Koltermann, L.M., Trunz, E., Schmulenson, E., Fritsch, A., Jaehde, U. & Fröhlich, H. (2025) Comparing scientific machine learning with population pharmacokinetic and classical machine learning approaches for prediction of drug concentrations. *CPT: Pharmacometrics & Systems Pharmacology* 14(4):759–769.
- Ahmadi Daryakenari, N., De Florio, M., Shukla, K. & Karniadakis, G.E. (2024) AI-Aristotle: a physics-informed framework for systems biology gray-box identification. *PLOS Computational Biology* 20(3):e1011916.
- Yang, L., Meng, X. & Karniadakis, G.E. (2021) B-PINNs: Bayesian physics-informed neural networks for forward and inverse PDE problems with noisy data. *Journal of Computational Physics* 425:109913.

A Full robustness tables

Table 4: Tissue RMSE (mg/L) across multiplicative noise levels ($n = 8, 5$ seeds). Best per row in bold.

σ	PINN	NLS	MLP
1%	0.024 ± 0.015	0.003 ± 0.002	0.382 ± 0.135
5%	0.029 ± 0.012	0.015 ± 0.012	0.366 ± 0.123
10%	0.039 ± 0.031	0.031 ± 0.025	0.355 ± 0.111
20%	0.109 ± 0.088	0.069 ± 0.064	0.370 ± 0.145

Table 5: Tissue RMSE (mg/L) across plasma sample counts ($\sigma = 10\%$, 5 seeds). Best per row in bold.

n	PINN	NLS	MLP
4	0.209 ± 0.074	0.047 ± 0.029	0.342 ± 0.066
6	0.069 ± 0.064	0.035 ± 0.028	0.374 ± 0.121
8	0.039 ± 0.031	0.031 ± 0.025	0.355 ± 0.111
12	0.042 ± 0.031	0.032 ± 0.029	0.352 ± 0.089
20	0.050 ± 0.027	0.033 ± 0.024	0.332 ± 0.083